Biophysical Journal Volume 108 February 2015 557–567

Article

Exact Stochastic Simulation of a Calcium Microdomain Reveals the Impact of Ca^{2+} Fluctuations on IP_3R Gating

Nicolas Wieder,[1,*] Rainer Fink,[1] and Frederic von Wegner[1]

[1]Medical Biophysics Unit, Department of Physiology and Pathophysiology, Universität Heidelberg, Heidelberg, Germany

ABSTRACT In this study, we numerically analyzed the nonlinear Ca^{2+}-dependent gating dynamics of a single, nonconducting inositol 1,4,5-trisphosphate receptor (IP_3R) channel, using an exact and fully stochastic simulation algorithm that includes channel gating, Ca^{2+} buffering, and Ca^{2+} diffusion. The IP_3R is a ubiquitous intracellular Ca^{2+} release channel that plays an important role in the formation of complex spatiotemporal Ca^{2+} signals such as waves and oscillations. Dynamic subfemtoliter Ca^{2+} microdomains reveal low copy numbers of Ca^{2+} ions, buffer molecules, and IP_3Rs, and stochastic fluctuations arising from molecular interactions and diffusion do not average out. In contrast to models treating calcium dynamics deterministically, the stochastic approach accounts for this molecular noise. We varied Ca^{2+} diffusion coefficients and buffer reaction rates to tune the autocorrelation properties of Ca^{2+} noise and found a distinct relation between the autocorrelation time τ_{ac}, the mean channel open and close times, and the resulting IP_3R open probability P_O. We observed an increased P_O for shorter noise autocorrelation times, caused by increasing channel open times and decreasing close times. In a pure diffusion model the effects become apparent at elevated calcium concentrations, e.g., at $[Ca^{2+}] = 25\ \mu M$, $\tau_{ac} = 0.082$ ms, the IP_3R open probability increased by $\approx$20% and mean open times increased by $\approx$4 ms, compared to a zero noise model. We identified the inactivating Ca^{2+} binding site of IP_3R subunits as the primarily noise-susceptible element of the De Young and Keizer model. Short Ca^{2+} noise autocorrelation times decrease the probability of Ca^{2+} association and consequently increase IP_3R activity. These results suggest a functional role of local calcium noise properties on calcium-regulated target molecules such as the ubiquitous IP_3R. This finding may stimulate novel experimental approaches analyzing the role of calcium noise properties on microdomain behavior.

INTRODUCTION

Ca^{2+} is a versatile second messenger, orchestrating a great variety of vital cellular functions such as cell motility (1), regulation of gene transcription (2), neurotransmitter release (3), and cytoskeleton dynamics (4). Its low intracellular resting concentration is maintained and tightly regulated by ion channels, ion pumps, and Ca^{2+} buffers (5). A central element of this regulation apparatus is the inositol 1,4,5-trisphosphate receptor (IP_3R), a large homotetrameric Ca^{2+} release channel protein accounting for Ca^{2+} flux from intracellular stores (endo-/sarcoplasmic reticulum) into the cytosol. It is regulated by IP_3, a second messenger produced by the membrane protein Phospholipase C, to transduce extracellular stimuli into intracellular Ca^{2+} signals. In addition to an IP_3 binding site, each of the four channel subunits has two Ca^{2+} binding sites that are responsible for the characteristic bell-shaped calcium response curve of IP_3R (6). While for low Ca^{2+} concentrations ($[Ca^{2+}]$) the high-affinity activating Ca^{2+} binding site accounts for the positive feedback mechanism known as calcium-induced calcium release, the low-affinity inactivating Ca^{2+} binding site induces a negative feedback mechanism, inactivating the IP_3 receptor at elevated $[Ca^{2+}]$ (7). IP_3Rs are not uniformly distributed. They are organized in channel clusters, each including a few tens of IP_3Rs and spaced 1–7 μm apart (8).

The synchronized openings of such clusters, carried by calcium-induced calcium release, are the foundation of experimentally observed elementary calcium release events called "calcium puffs" (9). Diffusion, the presence of Ca^{2+} pumps (e.g., SERCA), and Ca^{2+} buffers limit the spatiotemporal extent of these ECRE and control the coupling strength of adjacent IP_3R clusters. This quantization of Ca^{2+} signals in dynamic microdomains is the basis of more complex spatiotemporal signaling patterns such as calcium oscillations and calcium waves (10). It also introduces stochasticity into the process of signal generation. Microdomains only contain a small copy number of Ca^{2+} ions and IP_3Rs and therefore do not behave deterministically, which is reflected on a macroscopic level by spontaneous occurrences of Ca^{2+} puffs. It is now believed that global cellular Ca^{2+} signals are based on the stochastic occurrence of elementary calcium release events that, in turn, are carried by single channel noise (8,11–13).

These perceptions motivated the use of mathematical descriptions of Ca^{2+} signaling, which take into account the discrete and stochastic nature of molecular interactions (14,15). Consequently, a large number of simulation strategies for IP_3R-containing calcium microdomains have been proposed over the last decade (16,17). The fully stochastic

Submitted July 24, 2014, and accepted for publication November 18, 2014.

*Correspondence: nwieder@ix.urz.uni-heidelberg.de

Editor: Godfrey Smith.

0006-3495/15/02/0557/11 $2.00

http://dx.doi.org/10.1016/j.bpj.2014.11.3458

description of complex reaction-diffusion systems (RDS) is computationally demanding, and therefore most existing approaches implement hybrid algorithms. Hybrid algorithms are able to cover the hierarchical structure of calcium signals, spanning several orders of magnitude in space and time by treating functionally important nonlinear components such as the IP_3R stochastically, whereas passive bulk reactions and diffusion are treated deterministically (11,18–20). Because noise-induced effects on nonlinear systems have received special attention over the last few years (21–26), we chose a fully stochastic framework to investigate the effects of Ca^{2+} noise, arising from buffer association/dissociation reactions and diffusion, on the nonlinear behavior of IP_3Rs. Our model represents a Ca^{2+} microdomain with a single nonconducting IP_3R, integrating channel gating and Ca^{2+} dynamics in a common stochastic simulation framework based on Gillespie's algorithm. We started investigating the influence of pure diffusive Ca^{2+} noise on the nonlinear gating dynamics of the IP_3R, and then extended the model by introducing artificial Ca^{2+} buffers. In summary, we found that IP_3R gating is susceptible to Ca^{2+} noise in general, and to the Ca^{2+} noise autocorrelation time in particular.

MATERIALS AND METHODS

Stochastic description of chemical reaction diffusion systems

An exact stochastic description of chemical systems is provided by the chemical master equation (CME) (27). The CME describes the evolution of a chemical reaction system, comprised of a set of N molecular species $S = \{S_1,\ldots,S_N\}$, inside a system with volume Ω. The system state at time t is represented by the system state vector $\mathbf{x}(t) = (x_1(t),\ldots,x_N(t))$, where $x_k(t)$ denotes the molecular count of species S_k at time t. The system state is advanced by a set of M reaction events $R = \{R_1,\ldots,R_M\}$ that are defined as state change vectors $\mathbf{v}_j = (d_{j1},\ldots,d_{jN})$, $j = 1,\ldots,M$. Here d_{ji} represents the change in the molecular count of species S_i due to R_j. The CME reads as

$$\partial_t P(\boldsymbol{x},t) \;=\; \sum_{j=1}^{M}\left[a_j\left(\boldsymbol{x}-\boldsymbol{v}_j,t\right)P\left(\boldsymbol{x}-\boldsymbol{v}_j,t\right) - a_j(\boldsymbol{x},t)P(\boldsymbol{x},t)\right]$$

and states that the probability $P(\boldsymbol{x},t)$ of the system being at state $\boldsymbol{x}$ at time t is calculated from the net probability flow from state $\boldsymbol{x} - \boldsymbol{v}_j$ to $\boldsymbol{x}$, and vice versa. The propensity function $a_j(\boldsymbol{x},t)$ denotes the transition probability of R_j, given a system state $\boldsymbol{x}$ at time t. All these considerations are based on the basic assumption of a well-stirred chemical system, where nonreactive molecular collisions are far more likely than reactive events and exact positions, and velocities of single molecules are ignored (28).

It is possible to extend the CME to reaction diffusion systems by subdividing Ω into u smaller subvolumes (voxels) Ω_k, $k = 1,\ldots,u$. Subsequently, an additional spatial dimension is introduced into the CME, which leads to the reaction diffusion master equation (RDME) (29). This approach uses the classic CME in each voxel separately and connects the voxels by adding diffusion events to the set of state transitions R.

Gillespie's algorithm

For complex chemical reaction diffusion systems, the RDME quickly becomes analytically intractable. Gillespie's algorithm is a Monte Carlo procedure that simulates the time evolution of a system as a discrete multivariate Markov process (30). It is based on the joint probability density function

$$P(j,\tau|\boldsymbol{x},t) \;=\; a_j(\boldsymbol{x},t) \;\times\; \exp\left(-\sum_{j=1}^{M} a_j(\boldsymbol{x},t)\tau\right), \quad (1)$$

which determines the probability of state transition R_j to occur in the infinitesimal time interval $[t+\tau, t+\tau+\mathrm{d}\tau)$, given system state $\boldsymbol{x}$ at time t. The propensity functions $a_j(\boldsymbol{x},t)$ can be obtained from the deterministic reaction rate constants. In this study, we use the following.

1. First-order reactions. These are independent of the system volume Ω. Their propensity functions are directly proportional to the respective reaction rate constants $a_j(\boldsymbol{x},t) = k_j \times x_j(t)$.
2. Second-order reactions. They require molecular collisions of two educts, and therefore depend on Ω. We have $a_j(\boldsymbol{x},t) = k_j/\Omega \times h_j(\boldsymbol{x},t)$, where $h_j(\boldsymbol{x},t)$ denotes the number of unique reactant combinations at time t for R_j.
3. Diffusion events. These are characterized by a diffusion coefficient D and depend on the spatial extent of the considered system. Assuming a cubic simulation voxel with volume $\Omega = l^3$ and diffusion area $A = 6 \times l^2$, the propensity function reads $a_j(\boldsymbol{x},t) = D_j/l^2 \times x_j(t)$.

A rigorous derivation of these propensity functions has been presented by several authors before (31–33). One way of performing state transitions is the generation of exponentially distributed random waiting times τ_j for each R_j and executing the state transition with the minimum waiting time (first reaction method) (31). This requires the generation of M uniformly distributed random variables $r_1,\ldots,r_M$ and the computation of

$$\tau_j \;=\; \frac{-\log r_j}{a_j(\boldsymbol{x},t)}, \qquad j \;=\; 1,\ldots,M. \quad (2)$$

Let R_k be the state transition with the smallest associated τ_k. The system time t is then advanced to $t \rightarrow t+\tau_k$ and the system state is updated as $\boldsymbol{x}(t) \rightarrow \boldsymbol{x}(t) + \boldsymbol{v}_k$. The resulting simulation trajectories are exact solutions of the underlying RDME.

Many improvements to the classic version of Gillespie's algorithm have been proposed in the past (33). In this study, we use Gibson and Bruck's next reaction method (34). Its main advantages are the reuse of random numbers and the introduction of an optimized data structure.

Calcium buffer reactions

Ca^{2+} ions interact with a great variety of cytosolic buffer proteins (35):

$$Ca^{2+} + B \underset{k^-}{\overset{k^+}{\rightleftharpoons}} CaB. \quad (3)$$

Buffer molecules are characterized by their rate constants for association (k^+) and dissociation (k^-) reactions. The implementation of Ca^{2+} buffers to Gillespie's algorithm requires the definition of a second-order reaction for buffer association and a first-order reaction for the dissociation reaction. A summary of numerical values is given in Table 1.

Model geometry and diffusion

In this study, we consider a model consisting of a single simulation voxel surrounded by equilibrated boundary voxels, to account for diffusive transfer across the surface area as illustrated in Fig. 1 *A*. Inside the boundary voxels, we set all concentrations to their constant equilibrium concentrations and thus obtain a constant influx rate of diffusing molecular species (36). Introducing diffusion events considerably increases computation

TABLE 1 Model data

Reactant	K^+ (μM^{-1} ms^{-1})	k^- (ms^{-1})	K_d (μM)	D ($\mu m^2/s$)	c (μM)
Ca^{2+}	—	—	—	50–500	0.1–500
IP_3	—	—	—	0	10
B_1	0.01	0.1	10	0	300
B_2	0.05	0.5	10	0	300
B_3	0.1	1	10	0	300

Channel kinetics	Association (μM^{-1} ms^{-1})	Dissociation (ms^{-1})
IP_3 binding site	$a_1,a_3 = 0.08$	$b_1 = 6.4 \times 10^{-4}$
		$b_3 = 0.04$
Active Ca^{2+}	$a_5 = 0.015$	$b_5 = 0.012$
binding site	$a_2 = 4 \times 10^{-5}$	$b_2 = 4.8 \times 10^{-4}$
Inactive Ca^{2+}	$a_4 = 4 \times 10^{-4}$	$b_4 = 7.68 \times 10^{-5}$
binding site		
Subunit activation	$a_0 = 0.55$ ms^{-1}	$b_0 = 0.08$

Overview of system parameters used. We use IP_3R subunit transition rates as suggested by Rüdiger et al. (19) that were obtained from fitting experimental data from Mak et al. (7). The value k^+ is the buffer association reaction rate constant, k^- is the buffer dissociation reaction rate constant, and K_d is the respective buffer dissociation constant. D is the diffusion coefficient, and c is the concentration of the respective substance. Subunit state transition rates a_i,b_j refer to the De Young-Keizer model detailed in Fig. 1.

times. In this study, we only consider stationary Ca^{2+} buffers, limiting diffusion processes to Ca^{2+} ions. In all simulations, a cubic voxel geometry with box length $l = 0.5$ μm and thus $\Omega = 0.125$ fL is used.

Implementation of the IP_3R

A widely used gating scheme for the IP_3Rs is given by the eight-state subunit transition model proposed by De Young and Keizer in 1992 (37). It has been further refined by Shuai et al. (38), who introduced an additional active state that locks the subunits and prevents the dissociation of its ligands, reproducing experimentally observed ligand-independent channel flickering (39). Fig. 1 *B* illustrates the model with rate constants as proposed by Rüdiger et al. (19), shown in Table 1. Subunit state transition rates used in their study were obtained by fitting data from single channel recordings from Mak et al. (7) and are thus a solid foundation for the here presented simulations of an IP_3R. The three binding sites exposed by each subunit are represented by the numeration of the states where the first digit represents the IP_3 binding site, the second digit the activating Ca^{2+}, and the third digit the inactivating binding site. A value of 0 indicates a free binding site, whereas 1 represents an occupied binding site. The channel is considered to be in an open state whenever at least three subunits are in the active state [ACT]. If more than one IP_3R subunit has an occupied inactivating binding site ([IACT]), the channel is unable to open and thus considered to be completely inactivated.

In our implementation of Gillespie's algorithm, we consider each subunit state as a distinct molecular species. State transitions are implemented as second-order ligand binding reactions and first-order ligand dissociation reactions. The open channel is included as a further molecular species whereby its count is increased by 1 whenever at least three out of four subunits are active. Within this framework, the implementation of clusters of IP_3R channels as well as Ca^{2+}-conducting channels is straightforward. In this study, we only consider a single, nonconducting IP_3R, in analogy to experimental results from lipid bilayer studies (7).

As discussed earlier, simulation trajectories resulting from the here-used algorithm are exact. They are unevenly spaced time series of the system state, whereat each data point represents the system state after a single system state transition. It is therefore possible to track the exact points in time when the IP_3R opens or closes and the determination of channel open/close times is straightforward. Because no event is missed, the resulting statistical analysis of channel open/close times does not require correction.

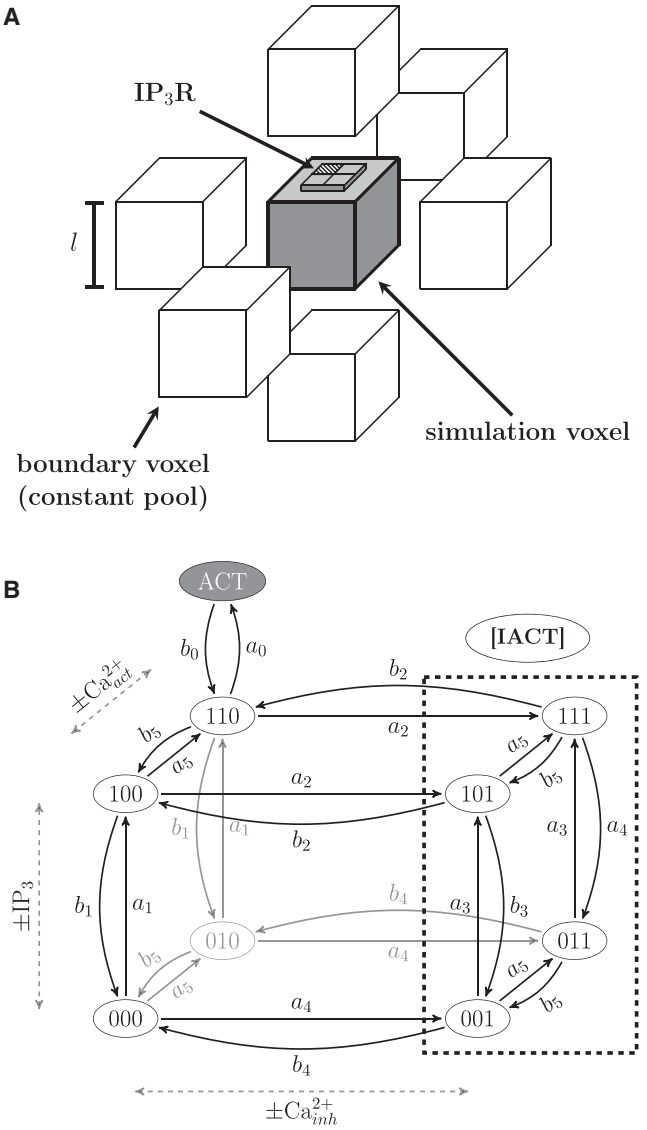

FIGURE 1 (*A*) Schematic illustration of the model geometry (*shaded box* in the *center*). Main simulation voxel, including a single IP_3R on top. Surrounding blank boxes represent the constant pool boundary voxel used in spatially resolved models. (*B*) De Young and Keizer state transition model of an IP_3R subunit (37) with an additional, ligand-independent [ACT] state (38). Four homotetrameric subunits form the channel protein that is in an open state whenever ≥ 3 subunits are active. A subunit exhibits three binding sites, represented by the numeration of the states. First digit, activating IP_3R binding site; second digit, activating Ca^{2+} binding site; third digit, inactivating Ca^{2+} binding site. Subunit states with an occupied inactivating Ca^{2+} binding site are summarized as inactive states ([IACT]) (*dashed box*). State transition rates are shown in Table 1 (19).

Characteristics of Ca^{2+} noise

All systems considered here obey combinatorial kinetics and, in the absence of channel flux, a constant detailed balanced equilibrium condition. The resulting Ca^{2+} noise distributions at equilibrium are therefore Poissonian (40) and for sufficiently large [Ca^{2+}], they are well approximated by a normally distributed random variable $\mathcal{N}(\mu,\sigma^2)$ with $\mu = \sigma^2$. In these cases, noise intensities at equilibrium depend solely on the mean [Ca^{2+}], and are independent from kinetic system properties. The resulting Ca^{2+} signal is stationary

and ergodic (41). In this study, we focus on the temporal characteristics of Ca^{2+} noise, in particular on the two-time autocorrelation function, which reveals information about properties of the underlying microscopic processes (42,43). By varying buffer reaction rates and diffusion coefficients, it is possible to tune the Ca^{2+} noise autocorrelation time (41). The autocorrelation function is well approximated by an exponentially decaying function (29,43,44) characterized by its decay rate τ_{ac}, which we will refer to as the "autocorrelation time" (Fig. 2). For a detailed theoretical analysis of the origins of Ca^{2+} fluctuations, the reader is referred to this recent publication (41).

Computation times

Simulations presented in this study were carried out on an Intel Core 2 Quad CPU Q9550 @ 2.83 GHz (Santa Clara, CA) and a cache size of 6144 Kb. Fig. 3 is based on data from simulation runs of at least 1.5×10^3 s for $[Ca^{2+}] = 0.1$–50 μM and at least 5×10^2 s for $[Ca^{2+}] = 100$–500 μM. Simulation times ranged from ~72 s to 6.5×10^5 s. RDS data presented in Figs. 4 and 5 result from simulation runs of at least 1×10^3 s. Here, simulation times ranged from ~10^3s to 4.5×10^4 s.

RESULTS

To study the noise susceptibility of a single, nonconducting IP_3R, we chose a saturating IP_3 concentration ($[IP_3]_{sat} = 10$ μM). In a first step, we used purely diffusive Ca^{2+} noise with varying diffusion coefficients to examine its influence on IP_3R gating dynamics over a range of $[Ca^{2+}] = 0.1$–500 μM. Consequently, we extended the system by introducing Ca^{2+} buffers and examined their additional influence on the IP_3R. In contrast to pure diffusion models that reveal constant Ca^{2+} noise τ_{ac} for different $[Ca^{2+}]$, the influence of a Ca^{2+} buffer on Ca^{2+} noise depends on its saturation level. With increasing buffer saturation, its influence decreases and noise characteristics are dominated by the remaining dynamic processes such as diffusion. Due to computational feasibility, the total buffer concentration $[B]_{tot}$ is limited in our models. To avoid buffer saturation phenomena, we therefore focused on a fixed $[Ca^{2+}] = 10$ μM and a Ca^{2+} buffer with dissociation constant $K_d = 10$ μM and constant $[B]_{tot} = 300$ μM. The choice of these model parameters

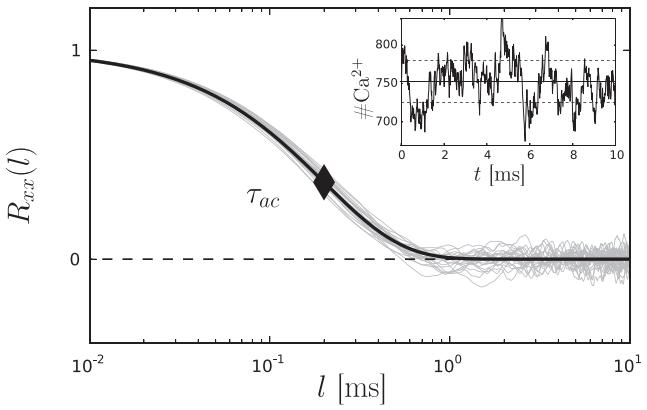

FIGURE 2 Estimated autocorrelation time of a plain diffusion system with $D_{Ca} = 200$ μm^2 s^{-1} and $[Ca^{2+}] = 10$ μM. Semilogarithmic representation of 20 exemplary autocorrelation functions $R_{xx}(l)$ (*shaded curves*) with exponential fit (*solid curve*) and a resulting autocorrelation time of $\tau_{ac} = 0.207$ ms (*solid diamond*). On the right, a representative simulation trajectory of purely diffusive Ca^{2+} noise with mean (*solid line*) and standard deviation (*dashed lines*) is shown ($T = 10$ ms).

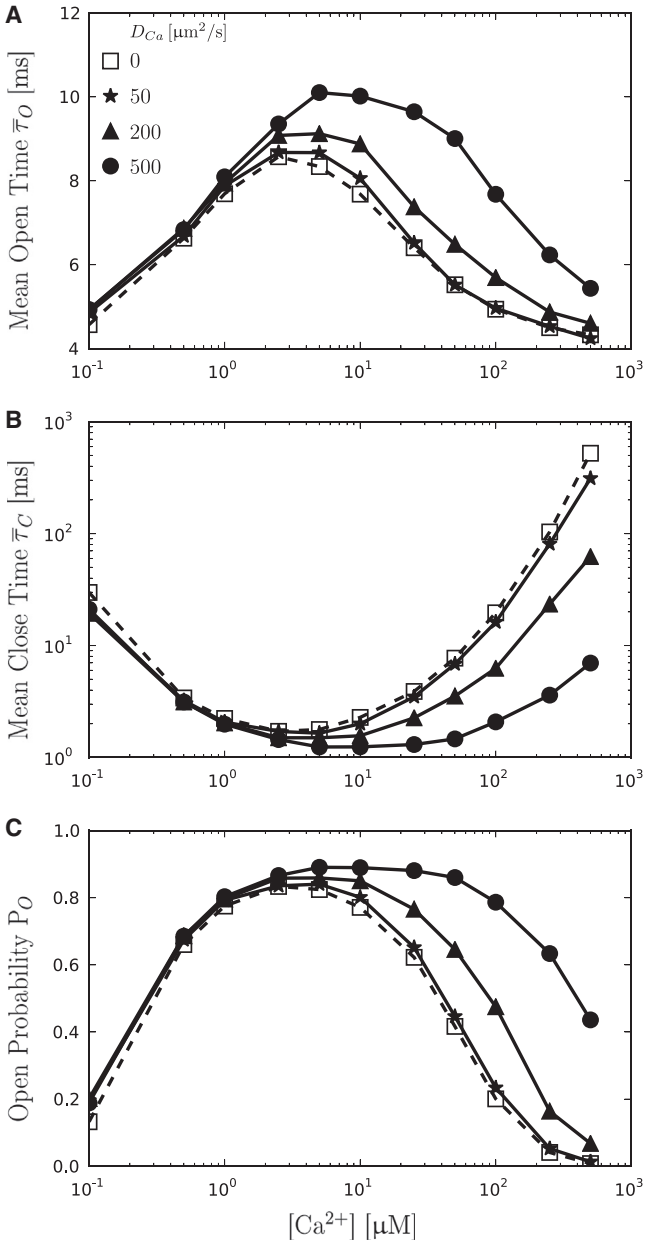

FIGURE 3 Summary of gating properties of the IP_3R for varying diffusion coefficients D_{Ca}. Open squares (*dashed curve*) are the result of zero noise models and represent the results expected from algorithms that treat Ca^{2+} dynamics deterministically. (*Solid curves*) Results for three different diffusion coefficients $D_{Ca} = 50$ μm^2 s^{-1} (*stars*), 200 μm^2 s^{-1} (*triangles*) and 500 μm^2 s^{-1} (*circles*). For low $[Ca^{2+}]$, Ca^{2+} noise has no obvious influence on the IP_3R. Starting at $[Ca^{2+}] = 1$ μM, (*A*) mean open times $\overline{\tau}_O$ increase with increasing D_{Ca}, whereas (*B*) mean close times $\overline{\tau}_C$ decrease. (*C*) Consequently, the channel open probability P_O increases with increasing D_{Ca}.

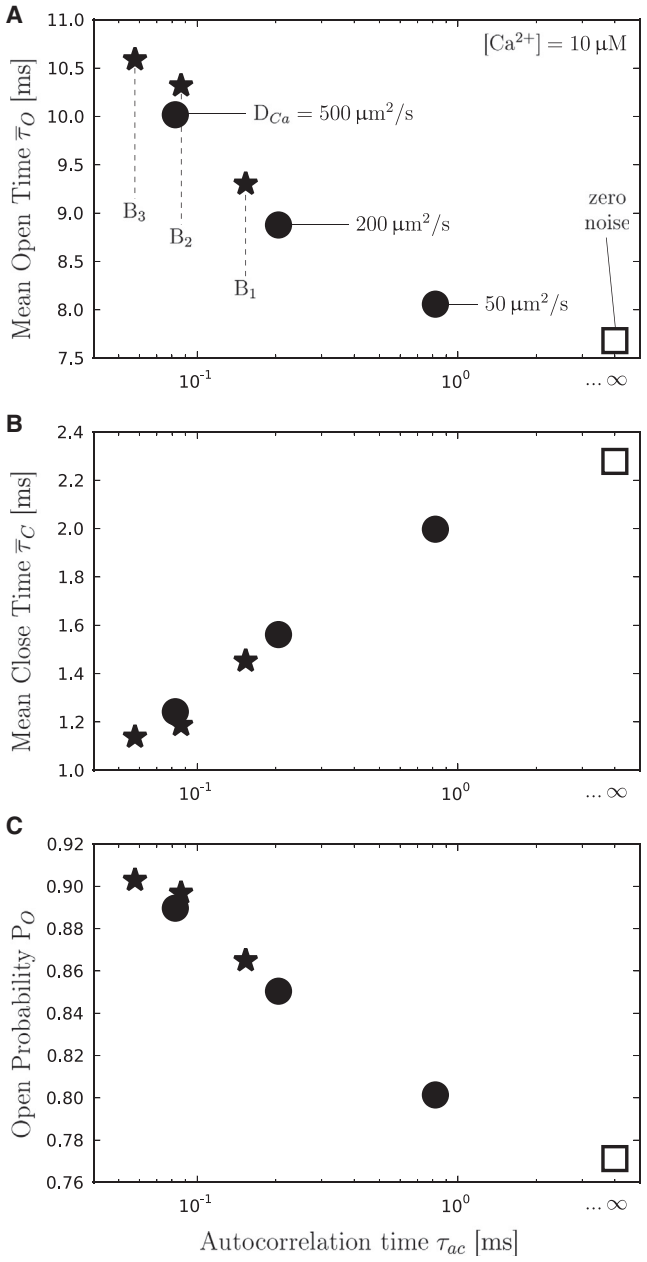

FIGURE 4 Summary of the relationship between IP$_3$R gating and τ_{ac} of Ca^{2+} noise at $[Ca^{2+}] = 10\ \mu M$. In addition to purely diffusive models (*circles*), results from a RDS with $D_{Ca} = 200\ \mu m^2\ s^{-1}$, including a single buffer with $K_d = 10\ \mu M$ and varying association reaction rates k^+ (see Table 1), are shown (*stars*). The zero noise model is included at an arbitrary *x*-intercept and represents a model with infinite τ_{ac} (*open square*). Mean open times $\overline{\tau}_O$ (*A*), mean close times $\overline{\tau}_C$ (*B*), and open probabilities P_O (*C*) are shown as a function of τ_{ac}.

reflects a compromise between a realistic Ca^{2+} buffer dissociation constant and an acceptable level of buffer saturation (50%). To vary temporal characteristics of Ca^{2+} noise, different on/off reaction rates have been used (see Table 1). All RDS models of the second part use a Ca^{2+} diffusion coefficient of $D_{Ca} = 200\ \mu m^2\ s^{-1}$.

The case of multibuffer systems can be effectively reduced to a single buffer system with a compound τ_{ac} (45). Temporal Ca^{2+} noise characteristics are dominated by the fastest present dynamic process involving Ca^{2+}. This means that a multibuffer system induces Ca^{2+} noise τ_{ac} comparable to a single buffer system, which only contains the fastest buffer (as long as the buffer is far from saturated).

IP$_3$R gating dynamics in a pure diffusion model

To investigate the noise susceptibility of the IP$_3$R, we used three different Ca^{2+} diffusion coefficients (D_{Ca} = 50 $\mu m^2\ s^{-1}$, 200 $\mu m^2\ s^{-1}$, and 500 $\mu m^2\ s^{-1}$) to introduce Ca^{2+} noise to the system. Channel dynamics are evaluated in terms of the mean open times $\overline{\tau}_O$, mean close times $\overline{\tau}_C$, and open probabilities P_O, for varying $[Ca^{2+}]$ = 0.1–500 μM. We included results from a zero noise model in order to compare with earlier results from hybrid models. The mean open/close times and open probabilities of the zero noise model are in good accordance with results from hybrid algorithms used by Shuai et al. (38) and Rüdiger et al. (19).

Fig. 3 summarizes the results and clearly shows that IP$_3$R gating dynamics are affected by Ca^{2+} noise. Ca^{2+} diffusion is modeled as a random walk between adjacent voxels (32) with a rate constant derived from the voxel geometry and the diffusion coefficient D_{Ca}. The corresponding τ_{ac} is equal to the inverse of the diffusion rate; therefore, increasing D_{Ca} leads to decreasing τ_{ac} (41). We found the estimated τ_{ac} from our simulations to be in good accordance with the expected values, as given in parentheses: For D_{Ca} = 50 $\mu m^2\ s^{-1}$, we found an autocorrelation time of $\tau_{ac}^{50} = 0.820 \pm 0.084$ ms (0.833 ms); for D_{Ca} = 200 $\mu m^2\ s^{-1}$, we found $\tau_{ac}^{200} = 0.204 \pm 0.021$ ms (0.208 ms); and for D_{Ca} = 500 $\mu m^2\ s^{-1}$, we found $\tau_{ac}^{500} = 0.082 \pm 0.0085$ ms (0.083 ms).

Because the noise variance is constant for fixed $[Ca^{2+}]$, noise-induced effects can be attributed to as the autocorrelation time of Ca^{2+} noise. Fig. 3 *A* shows that $\overline{\tau}_O$ increases for decreasing τ_{ac}. Ca^{2+} diffusion with D_{Ca} = 500 $\mu m^2\ s^{-1}$ shows a maximum of $\overline{\tau}_O$ = 10.07 ms ($[Ca^{2+}]$ = 5 μM) compared to the zero noise model with a maximum of $\overline{\tau}_O$ = 8.56 ms ($[Ca^{2+}]$ = 2.5 μM). Furthermore, short τ_{ac} values are associated with a delay of the negative Ca^{2+} feedback, and $\overline{\tau}_O$ remains on a high level, even for large $[Ca^{2+}]$. This effect is also shown in Fig. 3 *B*, where long $\overline{\tau}_C$ intervals, resulting from Ca^{2+}-dependent subunit inactivation, only appear at much larger $[Ca^{2+}]$ values as expected from the zero noise model. Fig. 3 *C* shows how the open probability P_O increases accordingly. While the zero noise model reveals a maximum P_O = 84% ($[Ca^{2+}]$ = 2.5 μM), the fast diffusion model shows a maximum of P_O = 89% ($[Ca2^+]$ = 10 μM). Open probabilities remained high even for large $[Ca^{2+}]$ when diffusive noise is considered.

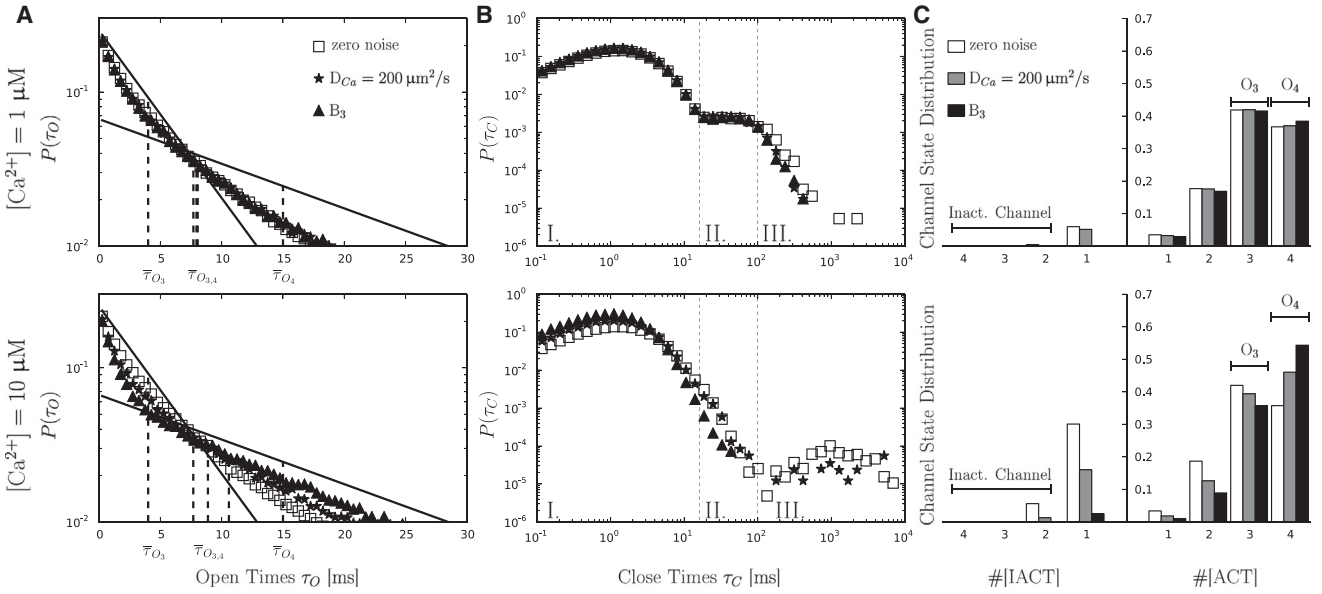

FIGURE 5 Open time distributions (*left column*), close time distributions (*middle column*) and subunit distributions (*right column*) at $[Ca^{2+}] = 1\ \mu M$ (*upper row*) and at $[Ca^{2+}] = 10\ \mu M$ (*lower row*). Results are shown for a zero noise model (*open squares*, *open bar*), pure diffusive noise with $D_{Ca} = 200\ \mu m^2\ s^{-1}$ (*stars, shaded bar*) and noise arising from a RDS including B_3 ($k^+ = 0.1\ \mu M^{-1}\ ms^{-1}$, $k^+ = 1\ ms^{-1}$) and diffusion with $D_{Ca} = 200\ \mu m^2\ s^{-1}$ (*triangles, solid bar*). (*A*) Expected open time distributions for O_3 and O_4 openings (*solid lines*) and the resulting biexponential open time distribution. (*Dashed lines*) Mean open times. (*B*) Within the close time distributions, we identify three distribution regions: Region I, channel closings resulting from channel flickering; Region II, channel closings resulting from a superposition of close states where the channel is not inactivated; and Region III, long close intervals resulting from channel inactivation. (*C*) Channel state distributions in terms of activated ([ACT]) and inactivated ([IACT]) subunits.

IP_3R gating dynamics in the vicinity of Ca^{2+} buffer

Introduction of Ca^{2+} buffer

To investigate the additional impact of Ca^{2+} buffers on Ca^{2+} noise and IP_3R gating, we simulated a RDS with a standard value of $D_{Ca} = 200\ \mu m^2\ s^{-1}$ (46) and an immobile Ca^{2+} buffer with $K_d = 10\ \mu M$. From Fig. 3, the clearest effects of Ca^{2+} noise on the IP_3R are expected for high $[Ca^{2+}]$. However, to avoid buffer saturation phenomena, we kept the $[Ca^{2+}]$ equilibrium concentration at $[Ca^{2+}]_{eq} = K_d = 10\ \mu M$. We obtained different τ_{ac} values by varying the buffer association rate k^+, keeping K_d constant. We used three different Ca^{2+} buffers B_1–B_3 (see Table 1 for numerical values) and found the corresponding Ca^{2+} noise τ_{ac} to be as follows: $\tau_{ac}^{(1)} = 0.153 \pm 0.035$ ms, $\tau_{ac}^{2} = 0.087 \pm 0.027$ ms, and $\tau_{ac}^{(3)} = 0.058 \pm 0.012$ ms.

In Fig. 4, mean channel open times $\overline{\tau}_O$, mean channel close times $\overline{\tau}_C$, and channel open probability P_O are shown as a function of Ca^{2+} noise τ_{ac}. In addition to the RDS models, we included the results from Fig. 3 to show that the impact on IP_3R gating is independent of the underlying noise generating mechanism. The zero noise model is included at an arbitrary x-intercept to represent a model with infinite τ_{ac}.

We found a dependency of $\overline{\tau}_O$, $\overline{\tau}_C$, and P_O on Ca^{2+} noise τ_{ac}. The decreasing τ_{ac} induced by Ca^{2+} buffers and diffusion leads to an increase in $\overline{\tau}_O$ and P_O, and to a decreasing $\overline{\tau}_C$. It is also observed that slow Ca^{2+} diffusion ($D_{Ca} = 50\ \mu m^2\ s^{-1}$) inducing relatively long Ca^{2+} noise τ_{ac} values has only very small effect on the IP_3R (see also Fig. 3).

Detailed channel gating analysis

Because the IP_3R opens whenever at least three out of four subunits are in the [ACT] state (see Fig. 1), it has two distinct open states. They can be distinguished by the maximum number of active subunits during an open interval, and are termed O_3 and O_4 (38). Data from patch-clamp experiments (47) and deterministic analysis of the IP_3R model (38) both reveal independent, exponential open time distributions for each open state. Our simulations reveal the same behavior, and we found dwell times for the O_3 and O_4 states that are in good accordance with previously published data (38), $\overline{\tau}_{O_3} \approx 4$ ms and $\overline{\tau}_{O_4} \approx 15$ ms. In contrast to only two open states, many more distinct close states exist (9^4–2). Mean close time distributions therefore show a more complex, multiexponential behavior. Nevertheless, it is possible to distinguish two major types of channel closings: 1) short close intervals, resulting from the ligand-independent inactivation of a single active subunit that underlies the typical channel flickering and 2) long close intervals that occur whenever Ca^{2+} binds to an inactivating binding site, accounting for the strong negative feedback at high $[Ca^{2+}]$.

While short closings only last for a few milliseconds, long close intervals can last up to seconds, and account for the burstlike opening pattern of IP_3Rs.

Fig. 5 shows a detailed channel gating analysis of three different models: a zero noise model, a purely diffusive noise model ($D_{Ca} = 200\ \mu m^2\ s^{-1}$), and an RDS model including the buffer B_3 ($k^+ = 0.1\ \mu M^{-1}\ ms^{-1}$, $k^- = 1\ ms^{-1}$), as well as Ca^{2+} diffusion ($D_{Ca} = 200\ \mu m^2\ s^{-1}$). The upper row shows results from models with $[Ca^{2+}] = 1\ \mu M$; the lower row shows results from models with $[Ca^{2+}] = 10\ \mu M$.

Open/close time distributions

Open time distributions are shown in the left column of Fig. 5. The biexponential decay results from the superposition of the open time distributions of O_3 and O_4 states (*solid lines*). Vertical dashed lines indicate the $\overline{\tau}_O$ value of the respective distribution. While the open time distribution for $[Ca^{2+}] = 1\ \mu M$ is unaffected by noise, we find a clear effect for $[Ca^{2+}] = 10\ \mu M$. A decreasing Ca^{2+} noise τ_{ac} induces a shift of the open time distributions toward the expected distribution for isolated O_4 openings. Mean open times $\overline{\tau}_O$ increase accordingly from 7.68 to 10.59 ms.

The middle column depicts the corresponding close time distributions. Based on theoretical mean waiting times $\overline{\tau}_w$ resulting from subunit transition rates, we subdivided the distributions roughly into three regions.

Region I. This distribution shows short channel closings, resulting from subunit transitions from [110] → [ACT] (channel flickering). This ligand-independent transition reveals a theoretical mean waiting time of $\overline{\tau}_w = 0.090$ ms.

Region II. This distribution is a superposition of close channel states with less than two inactivated subunits.

Region III. This distribution shows channel close states resulting from complete channel inactivation with more than one inactivated subunit. Assuming the IP_3R to be saturated with IP_3, the dissociation of Ca^{2+} from an inactivating Ca^{2+} binding site ([1x1] → [1x0]) reveals a theoretical mean waiting time $\overline{\tau}_w = 2083.3$ ms. The shape of the distribution changes from $[Ca^{2+}] = 1\ \mu M$ to $[Ca^{2+}] = 10\ \mu M$, where especially the fraction of prolonged close times increase for higher $[Ca^{2+}]$. This is mainly caused by increasing subunit inactivation, i.e., negative Ca^{2+} feedback. Again, noise only influences the close time distribution at $[Ca^{2+}] = 10\ \mu M$. The zero noise model shows a well-defined second peak in Region III, which slowly vanishes for decreasing τ_{ac}. Remarkably, the IP_3R does not completely inactivate at small τ_{ac} (*triangles*) values, explaining the large mean channel open times $\overline{\tau}_O$ in Fig. 3. Consequently, mean channel close times $\overline{\tau}_C$ decrease with decreasing τ_{ac} from 2.28 to 1.14 ms (Fig. 4 *B*).

Channel state distribution

The right column of Fig. 5 shows the channel state distribution as histograms. Because the IP_3R consists of four subunits with nine different subunit states each, the resulting total number of possible channel states is $9^4 = 6561$. Here, we simplify the situation by defining a state solely by its number of active ([ACT]) or inactive ([IACT]) subunits (see Fig. 1). The right side of Fig. 5 *C* shows the channel state distribution in terms of the number of [ACT] subunits, the left side in terms of the number of [IACT] subunits. For $[Ca^{2+}] = 1\ \mu M$, the average number of [ACT] states are insusceptible to noise and average numbers of [IACT] differ only slightly. Invariant open time distributions go along with a nearly constant ratio of O_3/O_4 openings (≈ 1.14).

It is also observed that complete channel inactivation ([IACT] > 1) occurs very rarely, leading to invariant close time distributions. In contrast, the histogram for $Ca^{2+} = 10\ \mu M$ shows a strong, τ_{ac}-dependent deviation from this pattern. The O_3/O_4 ratio varies considerably ranging from 0.67 in RDS models to 1.17 in zero noise models, explaining the skewed open time distributions. With increasing $[Ca^{2+}]$, subunit inactivation becomes more likely and we find an increased fraction of inactivated channel states ([IACT] > 1). However, noise also influences channel inactivation. While the zero noise model reveals a fraction of 5% inactivated channels, this value decreases to 1.5% for the purely diffusive noise model, and vanishes for the RDS model. The channel state distribution explains the vanishing peak in Region III of the close time distribution for decreasing Ca^{2+} noise τ_{ac}.

In summary, we can explain the initially observed, noise-induced alteration of mean channel open times $\overline{\tau}_O$, mean channel close times $\overline{\tau}_C$, and open probabilities P_O with a shift in the channel state distribution away from inactivated states and toward the O_4 open states.

DISCUSSION

Our motivation to study the influence of Ca^{2+} noise on the IP_3R arose from the contemporary interest in the stochastic nature of complex Ca^{2+} signals (11,20,26,41). Just recently, Thurley et al. (13) showed that stimulus intensities of input signals are reliably encoded in stochastic sequences of random spikes, and the body of literature, emphasizing the functional relevance of noise in biological systems, is constantly growing (24,48–52).

The exact stochastic description of chemical RDS is universal and therefore, models of arbitrary complexity can be implemented in a consistent framework. However, running the model can be computationally demanding and in practice, the spatio-temporal dimensions of realistic models are limited. An alternative modeling strategy is represented by hybrid algorithms that treat nonlinear system components stochastically and bulk reactions deterministically (11,19,38,53–55). In terms of Ca^{2+} signaling, hybrid approaches explicitly ignore Ca^{2+} noise.

As noise-induced effects on nonlinear systems have received much interest over the past years (21,56), we designed a reduced, computationally feasible, fully stochastic

model of a Ca^{2+} microdomain, to investigate the influence of Ca^{2+} noise on IP_3R gating dynamics.

We observed that the Ca^{2+} noise autocorrelation time τ_{ac} has a significant effect on mean open times, mean close times, and the open probability of the IP_3R (see Fig. 4). As shown in Fig. 3, the effect becomes apparent for $[Ca^{2+}] > 1\ \mu M$ and mainly affects channel inactivation. This is confirmed in Fig. 5, where open and close time distributions are noise-invariant for $[Ca^{2+}] = 1\ \mu M$, whereas the distributions are clearly skewed for $[Ca^{2+}] = 10\ \mu M$. The corresponding channel state histograms emphasize that decreasing τ_{ac} induces a shift in the channel state distribution from [IACT] toward [ACT], decreasing channel inactivation and stabilizing channel open states. Our data shows that Ca^{2+} noise reduces the probability for subunit inactivation, which in turn increases the number of [ACT] subunit states and consequently the number of O_4 openings. At $[Ca^{2+}] = 10\ \mu M$, for example, the proportion of inactivating subunit state transitions was $\approx 0.35\%$ for the zero noise model, $\approx 0.18\%$ for the pure diffusive model, and $\approx 0.07\%$ for the RDS model. Subunit inactivations are rare events compared to channel openings, but with a strong impact on the IP_3R channel state distribution. A single inactivated subunit prevents O_4 openings for a duration up to seconds, and two inactive subunits prevent the IP_3R completely from opening. Therefore, minimal changes in the channel inactivation probability lead to significant changes of mean channel open/close times and open probabilities.

Both the functionally important association of Ca^{2+} to the activating binding site and the inactivating binding site are second-order reactions. The influence of fluctuations in the educt species of simple second-order reactions has been studied analytically by Morita (57) and Katsumoto and Morita (58) in closed systems. They showed in their work that fluctuations not only alter equilibrium concentrations but also influence the dynamics of the reaction. The here used gating scheme of IP_3R subunits consists of eight interconnected, Ca^{2+}-dependent second-order reactions and exponentially correlated Ca^{2+} noise (compared to uncorrelated noise in Morita and Katsumo's work). The situation here is therefore much more complex, and a rigorous physical explanation for the observed effects would require an analytically solution of the proposed model. But an analytical solution is, to the best of our knowledge, not available at the moment. We can therefore only hypothesize about the origin of the noise-induced delay of subunit inactivation. Fig. 6 shows the distributions of the most frequent subunit states ([ACT], [IACT], [110]) as a function of $[Ca^{2+}]$, whereby the shaded curve represents the zero noise model and the solid curve a purely diffusive model ($D_{Ca} = 200\ \mu m^2\ s^{-1}$).

It becomes clear that subunit activation and inactivation does not follow the binding curves expected from the rate constants of the respective binding sites. This shift can be

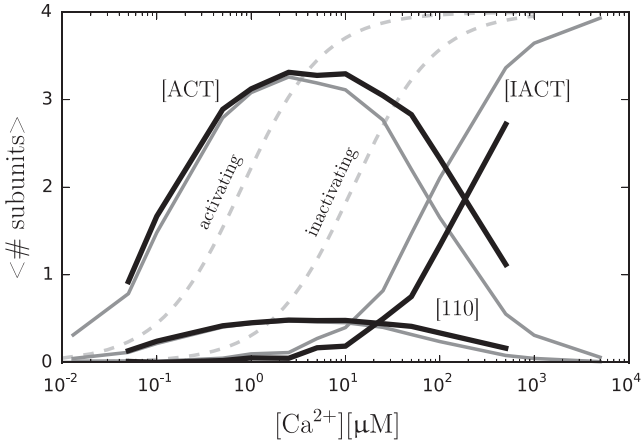

FIGURE 6 Subunit distribution of the three most frequent subunit states [ACT], [IACT], and [110] are shown as a function of $[Ca^{2+}]$. The distributions of the zero noise model (*shaded curve*) and a pure diffusion model with $D_{Ca} = 200\ \mu m^2\ s^{-1}$ (*solid curve*) are shown. As a reference, isolated binding curves of the activating and inactivating binding site are shown (*light-shaded dashed curves*). Note that due to crucially shorter computation times, data of the zero noise model is available for a greater range of $[Ca^{2+}]$ than for the diffusive model.

attributed to the ligand-independent subunit activation transition that locks [110] subunits with a high rate. The binding curve of the activating binding site is therefore shifted to lower $[Ca^{2+}]$, while the binding curve for the inactivating binding site is shifted to higher $[Ca^{2+}]$. This effect explains the late inactivation of channel subunits, even for the zero noise model. Ca^{2+} noise, here introduced by diffusion, clearly shifts the binding curve of the inactivating site further to higher $[Ca^{2+}]$, while leaving the binding curve of the activating binding site mainly unaffected. There are three main differences between the two Ca^{2+} binding sites that could serve as an explanation for this behavior: 1) the activating binding site has a much higher association rate than the inactivating binding site; 2) the dissociation constants of the two binding sites differ by a factor of 10; and 3) the lockable subunit [110] is a product of subunit activation, while it is an educt for subunit inactivation.

The consequent examination of the influence of these differences on the noise susceptibility of IP_3Rs would go beyond the scope of this study. However, future investigations should be directed toward this problem to gain a deeper understanding of the effect of Ca^{2+} noise on the nonlinear dynamics of the De Young and Keizer subunit transition model for IP_3Rs.

The biphasic Ca^{2+} feedback of the IP_3R is the functional basis of Ca^{2+} waves and oscillations (59). Noise-induced delay of negative Ca^{2+} feedback therefore affects the fundamental mechanism of spatiotemporal Ca^{2+} signal formation. We showed that not only diffusion, but also the presence of Ca^{2+} buffers shape the temporal properties of Ca^{2+} fluctuations and consequently IP_3R gating. The influence of Ca^{2+} buffers on Ca^{2+} signaling has previously been

studied, both theoretically (54,60–62) and experimentally (63–66). These studies mainly focused on the influence of mobile and immobile buffers on global Ca^{2+} signals, whereas only a very few studies are concerned with the functional role of buffer-dependent Ca^{2+} fluctuations (26). The expression profiles for Ca^{2+} buffers with widely differing kinetic properties are highly variable among different cell types (35,46).

There is a large number of naturally occurring Ca^{2+} buffers and their dissociation constants range from only a few nM (e.g., α-Parvalbumin, $K_d = 4$–9 nM (35)) to up to tens of μM (e.g., α-Secretagogin, $K_d = 25$ μM (67)). Furthermore, there are slow (e.g., α-Parvalbumin, $k^+ = 1 \times 10^{-3}$ μM^{-1} ms^{-1}) and fast Ca^{2+} buffers (e.g., Calbindin-D9k, $k^+ = 1$ μM^{-1} ms^{-1}), as characterized by their Ca^{2+} association rates k^+. Specific buffer expression profiles may therefore constitute a powerful tool that allows the cell to influence Ca^{2+} signaling on different levels, ranging from the modulation of stochastic Ca^{2+} fluctuations up to the spatiotemporal modulation of ECRE, waves, and oscillations. Another thought should be dedicated to the fact that most experimental settings include artificial Ca^{2+} buffers, either to control $[Ca^{2+}]$ or in the form of fluorescent Ca^{2+} dyes. The range of physico-chemical properties of artificial Ca^{2+} buffers adds to the complexity of the problem (68). As we have shown in this study, artificial Ca^{2+} buffers may significantly alter the properties of calcium noise and possibly, the behavior of the observed calcium microdomain.

So far, we have only investigated the noise susceptibility of the IP_3R in silico. We used the nine-state De Young-Keizer subunit state transition model as proposed by Shuai et al. (38) with parameters from Rüdiger et al. (19). In accordance with structural and mutational studies (69), the model assumes that the IP_3R consists of four identical subunits with an IP_3-binding site, an activating Ca^{2+} binding site and an inactivating Ca^{2+} binding site (70). The originally proposed eight-state De Young-Keizer model (37) was extended by a ligand-independent [ACT] state in order to account for experimental observations including channel flickering (39) and calcium-independence of the activated open state (38,71). Following other studies showing the functional relevance of noise experimentally (20,72–74), our findings await experimental verification.

For instance, an IP_3R channel incorporated into a lipid bilayer could be exposed to a defined calcium microenvironment. This setting should allow for the observation of IP_3R gating in a controlled Ca^{2+}-buffer system. Statistical properties of Ca^{2+} noise and the corresponding two-time correlation function in particular could be measured with fluorescence correlation spectroscopy (75). This approach would allow to investigate experimentally the influence of both natural Ca^{2+} buffers and widely used fluorescence dyes on Ca^{2+} fluctuations and IP_3R gating. A further interesting focus for future investigations is the noise susceptibility of the ryanodine receptor, structurally closely related to the IP_3R and representing the main Ca^{2+} release channel in cardiac and striated muscle cells (76). Due to a similar biphasic Ca^{2+} dependency, a similar influence of stochastic Ca^{2+} fluctuations on the gating behavior of the ryanodine receptor is expected (77).

To understand our findings in the global context of Ca^{2+} signaling, it is necessary to extend our models to clusters of IP_3R channels, and beyond. Furthermore, it is necessary to consider Ca^{2+} flux through the channel pore, because it has been shown that the magnitude of Ca^{2+} fluctuations reveals a dependency on total buffer concentration and buffer kinetics in systems with constant Ca^{2+} influx (41). Because our model and software framework are capable of simulating both channel clusters and Ca^{2+} flux, the investigation of more complex models will be the subject of future investigations (14,15,17,36).

The spatial extent of our models is so far also limited by computational feasibility. A more efficient strategy would be the approximation of the CME by a Fokker-Planck equation or a chemical Langevin equation (78) but there are limitations to find a satisfactory approximation, namely the existence of a macroscopically infinitesimal time domain (79). An adequate approximation requires the existence of a time interval during which changes in the propensity functions are negligibly small, whereas each state transition is expected to occur sufficiently frequently ($n >> 1$). Given the model parameters used in this study, this condition is not met, mainly due to the large timescale of IP_3R subunit state transitions and the low copy number of both Ca^{2+} ions and IP_3Rs. The rarely occurring and functionally essential Ca^{2+}-dependent channel inactivation constitutes the limiting factor.

Ca^{2+} microdomains are a fundamental entity of Ca^{2+}-mediated cell functions (80). Morphologically predetermined structures, such as neuronal dendritic spines or the dyadic cleft of cardiac myocytes, are prominent examples for their vital roles in learning, memory (81), and heartbeat generation (82). Even though some recent work about stochastic fluctuations in the dyadic cleft exists (26), the question how such fluctuations influence the Ca^{2+} signaling apparatus as a whole, remains unanswered.

Beyond the scope of Ca^{2+} signaling, our work illustrates the important role of mesoscopic chemical noise for intracellular signaling networks. Nonlinearities such as allosteric regulation, positive and negative feedback mechanisms, and covalent modifications are ubiquitous and low-copy numbers of key molecules appear frequently. In these situations it is necessary to recognize noise as an active element within biological signaling networks.

REFERENCES

1. Wei, C., X. Wang, …, H. Cheng. 2012. Calcium gradients underlying cell migration. *Curr. Opin. Cell Biol.* 24:254–261.

2. Dolmetsch, R. E., K. Xu, and R. S. Lewis. 1998. Calcium oscillations increase the efficiency and specificity of gene expression. *Nature.* 392:933–936.
3. Südhof, T. C. 2012. Calcium control of neurotransmitter release. *Cold Spring Harb. Perspect. Biol.* 4:a011353.
4. Greka, A., and P. Mundel. 2012. Calcium regulates podocyte actin dynamics. *In* Seminars in Nephrology, *Vol. 32*.. Elsevier, New York, pp. 319–326.
5. Berridge, M. J., M. D. Bootman, and H. L. Roderick. 2003. Calcium signaling: dynamics, homeostasis and remodeling. *Nat. Rev. Mol. Cell Biol.* 4:517–529.
6. Bezprozvanny, l., J. Watras, and B. E. Ehrlich. 1991. Bell-shaped calcium-response curves of $Ins_{l,4,5}P_3$- and calcium-gated channels from endoplasmic reticulum of cerebellum. *Nature.* 351:751–754.
7. Mak, D. O., S. McBride, and J. K. Foskett. 1998. Inositol 1,4,5-trisphosphate [correction of tris-phosphate] activation of inositol trisphosphate [correction of tris-phosphate] receptor Ca^{2+} channel by ligand tuning of Ca^{2+} inhibition. *Proc. Natl. Acad. Sci. USA.* 95:15821–15825.
8. Skupin, A., H. Kettenmann, …, M. Falcke. 2008. How does intracellular Ca^{2+} oscillate: by chance or by the clock? *Biophys. J.* 94:2404–2411.
9. Parker, I., and Y. Yao. 1991. Regenerative release of calcium from functionally discrete subcellular stores by inositol trisphosphate. *Proc. Biol. Sci.* 246:269–274.
10. Marchant, J. S., and I. Parker. 2001. Role of elementary Ca^{2+} puffs in generating repetitive Ca^{2+} oscillations. *EMBO J.* 20:65–76.
11. Skupin, A., H. Kettenmann, and M. Falcke. 2010. Calcium signals driven by single channel noise. *PLOS Comput. Biol.* 6:e1000870t.
12. Skupin, A., and M. Falcke. 2009. From puffs to global Ca^{2+} signals: how molecular properties shape global signals. *Chaos.* 19:037111.
13. Thurley, K., S. C. Tovey, …, M. Falcke. 2014. Reliable encoding of stimulus intensities within random sequences of intracellular Ca^{2+} spikes. *Sci. Signal.* 7:ra59.
14. Wieder, N., R. H. A. Fink, and F. von Wegner. 2012. Mesoscopic simulation of subcellular calcium microdomains and calcium-regulated calcium channels. *In* Calcium Channels: Properties, Functions and Regulation. M. R. Figgins, editor. Nova Science Publishers, Hauppauge, NY, pp. 121–136.
15. von Wegner, F., N. Wieder, and R. H. Fink. 2012. Simulation strategies for calcium microdomains and calcium-regulated calcium channels. *In* Calcium Signaling. S. Islam, editor. Springer, New York, pp. 553–567.
16. Dupont, G., L. Combettes, …, J. W. Putney. 2011. Calcium oscillations. *Cold Spring Harb. Perspect. Biol.* 3:a004226w.
17. Wieder, N., R. H. A. Fink, and Fv. Wegner. 2011. Exact and approximate stochastic simulation of intracellular calcium dynamics. *J. Biomed. Biotechnol.* 2011:572492.
18. Swillens, S., P. Champeil, …, G. Dupont. 1998. Stochastic simulation of a single inositol 1,4,5-trisphosphate-sensitive Ca^{2+} channel reveals repetitive openings during 'blip-like' Ca^{2+} transients. *Cell Calcium.* 23:291–302.
19. Rüdiger, S., J. W. Shuai, …, M. Falcke. 2007. Hybrid stochastic and deterministic simulations of calcium blips. *Biophys. J.* 93:1847–1857.
20. Dupont, G., A. Abou-Lovergne, and L. Combettes. 2008. Stochastic aspects of oscillatory Ca^{2+} dynamics in hepatocytes. *Biophys. J.* 95:2193–2202.
21. Longtin, A. 2003. Effects of noise on nonlinear dynamics. *In* Nonlinear Dynamics in Physiology and Medicine. A. Beuter, L. Glass, M. C. Mackey, and M. S. Titcombe, editors. Springer, New York, pp. 149–189.
22. Li, Q. S., and P. Wang. 2004. Internal signal stochastic resonance induced by colored noise in an intracellular calcium oscillations model. *Chem. Phys. Lett.* 387:383–387.
23. Blomberg, C. 2006. Fluctuations for good and bad: the role of noise in living systems. *Phys. Life Rev.* 3:133–161.
24. Faisal, A. A., L. P. J. Selen, and D. M. Wolpert. 2008. Noise in the nervous system. *Nat. Rev. Neurosci.* 9:292–303.
25. Simpson, M., C. Cox, …, J. Cooke. 2009. Noise in biological circuits. *WIREs Nanomed. Nanobiotechnol.* 1:214–225.
26. Weinberg, S. H., and G. D. Smith. 2012. Discrete-state stochastic models of calcium-regulated calcium influx and subspace dynamics are not well-approximated by ODEs that neglect concentration fluctuations. *Comput. Math. Methods Med.* 2012:897371.
27. Gillespie, D. T. 1992. A rigorous derivation of the chemical master equation. *Phys. A (Amsterdam, Neth.).* 188:404–425.
28. Gillespie, D. T. 2007. Stochastic simulation of chemical kinetics. *Annu. Rev. Phys. Chem.* 58:35–55.
29. Malek-Mansour, M., and G. Nicolis. 1975. A master equation description of local fluctuations. *J. Stat. Phys.* 13:197–217.
30. Gillespie, D. T. 1977. Exact stochastic simulation of coupled chemical reactions. *J. Phys. Chem. A.* 81:2340–2361.
31. Gillespie, D. T. 1976. A general method for numerically simulating the stochastic time evolution of coupled chemical reactions. *J. Comput. Phys.* 22:403–434.
32. Elf, J., A. Doncic, and M. Ehrenberg. 2003. Mesoscopic reaction-diffusion in intracellular signaling. *In* SPIE's First International Symposium on Fluctuations and Noise. International Society for Optics and Photonics (SPIE), Bellingham, WA, pp. 114–124.
33. Gillespie, D. T., A. Hellander, and L. R. Petzold. 2013. Perspective: stochastic algorithms for chemical kinetics. *J. Chem. Phys.* 138: 170901.
34. Gibson, M. A., and J. Bruck. 2000. Efficient exact stochastic simulation of chemical systems with many species and many channels. *J. Phys. Chem. A.* 104:1876–1889.
35. Schwaller, B. 2010. Cytosolic Ca^{2+} buffers. *Cold Spring Harb. Perspect. Biol.* 2:a004051.
36. von Wegner, F., and R. H. A. Fink. 2010. Stochastic simulation of calcium microdomains in the vicinity of an L-type calcium channel. *Eur. Biophys. J.* 39:1079–1088.
37. De Young, G. W., and J. Keizer. 1992. A single-pool inositol 1,4,5-trisphosphate-receptor-based model for agonist-stimulated oscillations in Ca^{2+} concentration. *Proc. Natl. Acad. Sci. USA.* 89:9895–9899.
38. Shuai, J., J. E. Pearson, …, I. Parker. 2007. A kinetic model of single and clustered IP_3 receptors in the absence of Ca^{2+} feedback. *Biophys. J.* 93:1151–1162.
39. Mak, D.-O. D., S. M. McBride, and J. K. Foskett. 2003. Spontaneous channel activity of the inositol 1,4,5-trisphosphate ($InsP_3$) receptor ($InsP_3R$). Application of allosteric modeling to calcium and $InsP_3$ regulation of $InsP_3R$ single-channel gating. *J. Gen. Physiol.* 122:583–603.
40. Gardiner, C., and S. Chaturvedi. 1977. The Poisson representation. I. A new technique for chemical master equations. *J. Stat. Phys.* 17:429–468.
41. Weinberg, S. H., and G. D. Smith. 2014. The influence of Ca^{2+} buffers on free $[Ca^{2+}]$ fluctuations and the effective volume of Ca^{2+} microdomains. *Biophys. J.* 106:2693–2709.
42. Elson, E. L., and D. Magde. 1974. Fluorescence correlation spectroscopy. I. Conceptual basis and theory. *Biopolymers.* 13:1–27.
43. Gardiner, C., K. McNeil, …, I. Matheson. 1976. Correlations in stochastic theories of chemical reactions. *J. Stat. Phys.* 14:307–331.
44. Hänggi, P., and P. Jung. 1995. Colored noise in dynamical systems. *Adv. Chem. Phys.* 89:239–326.
45. von Wegner, F., N. Wieder, and R. H. Fink. 2014. Microdomain calcium fluctuations as a colored noise process. *Front. Genet.* 5:376.
46. Schwaller, B. 2009. The continuing disappearance of "pure" Ca^{2+} buffers. *Cell. Mol. Life Sci.* 66:275–300.
47. Mak, D.-O. D., and J. K. Foskett. 1997. Single-channel kinetics, inactivation, and spatial distribution of inositol trisphosphate (IP_3) receptors in *Xenopus* oocyte nucleus. *J. Gen. Physiol.* 109:571–587.
48. Hänggi, P. 2002. Stochastic resonance in biology. How noise can enhance detection of weak signals and help improve biological information processing. *ChemPhysChem.* 3:285–290.

49. Elowitz, M. B., A. J. Levine, …, P. S. Swain. 2002. Stochastic gene expression in a single cell. *Science.* 297:1183–1186.
50. Raj, A., and A. van Oudenaarden. 2008. Nature, nurture, or chance: stochastic gene expression and its consequences. *Cell.* 135:216–226.
51. McDonnell, M. D., and D. Abbott. 2009. What is stochastic resonance? Definitions, misconceptions, debates, and its relevance to biology. *PLOS Comput. Biol.* 5:e1000348.
52. Wilkinson, D. J. 2009. Stochastic modeling for quantitative description of heterogeneous biological systems. *Nat. Rev. Genet.* 10:122–133.
53. Falcke, M. 2003. On the role of stochastic channel behavior in intracellular Ca^{2+} dynamics. *Biophys. J.* 84:42–56.
54. Shuai, J., J. E. Pearson, and I. Parker. 2008. Modeling Ca^{2+} feedback on a single inositol 1,4,5-trisphosphate receptor and its modulation by Ca^{2+} buffers. *Biophys. J.* 95:3738–3752.
55. Moenke, G., M. Falcke, and K. Thurley. 2012. Hierarchic stochastic modeling applied to intracellular Ca^{2+} signals. *PLoS ONE.* 7:e51178.
56. Mosconi, F., T. Julou, …, D. Bensimon. 2008. Some nonlinear challenges in biology. *Nonlinearity.* 21:T131.
57. Morita, A. 1988. Externally driven fluctuation of concentration and dynamics of second order chemical reaction. *J. Chem. Phys.* 88:7481–7484.
58. Katsumoto, M., and A. Morita. 1989. Externally driven fluctuation of concentration in the second-order chemical reaction and the dynamic fluctuation increase. *J. Chem. Soc., Faraday Trans.* 85:623–633.
59. Brandman, O., and T. Meyer. 2008. Feedback loops shape cellular signals in space and time. *Science.* 322:390–395.
60. Fraiman, D., and S. P. Dawson. 2014. Buffer regulation of calcium puff sequences. *Phys. Biol.* 11:016007.
61. Rüdiger, S., Ch. Nagaiah, …, J. W. Shuai. 2010. Calcium domains around single and clustered IP_3 receptors and their modulation by buffers. *Biophys. J.* 99:3–12.
62. Sneyd, J., P. D. Dale, and A. Duffy. 1998. Traveling waves in buffered systems: applications to calcium waves. *SIAM J. Appl. Math.* 58:1178–1192.
63. Jackson, M. B., and S. J. Redman. 2003. Calcium dynamics, buffering, and buffer saturation in the boutons of dentate granule-cell axons in the hilus. *J. Neurosci.* 23:1612–1621.
64. Ricci, A. J., Y. C. Wu, and R. Fettiplace. 1998. The endogenous calcium buffer and the time course of transducer adaptation in auditory hair cells. *J. Neurosci.* 18:8261–8277.
65. Kreiner, L., and A. Lee. 2006. Endogenous and exogenous Ca^{2+} buffers differentially modulate Ca^{2+}-dependent inactivation of $Ca_v2.1$ Ca^{2+} channels. *J. Biol. Chem.* 281:4691–4698.
66. Matthews, E. A., S. Schoch, and D. Dietrich. 2013. Tuning local calcium availability: cell-type-specific immobile calcium buffer capacity in hippocampal neurons. *J. Neurosci.* 33:14431–14445.
67. Alpár, A., J. Attems, …, T. Harkany. 2012. The renaissance of Ca^{2+}-binding proteins in the nervous system: secretagogin takes center stage. *Cell. Signal.* 24:378–387.
68. Johnson, I. D. 2010. The Molecular Probes Handbook—A Guide to Fluorescent Probes and Labeling Technologies. Life Technologies, Norwalk, CT.
69. Foskett, J. K., C. White, …, D.-O. D. Mak. 2007. Inositol trisphosphate receptor Ca^{2+} release channels. *Physiol. Rev.* 87:593–658.
70. Taylor, C. W., and S. C. Tovey. 2010. IP_3 receptors: toward understanding their activation. *Cold Spring Harb. Perspect. Biol.* 2:a004010.
71. Adkins, C. E., and C. W. Taylor. 1999. Lateral inhibition of inositol 1,4,5-trisphosphate receptors by cytosolic Ca^{2+}. *Curr. Biol.* 9:1115–1118.
72. Dorval, Jr., A. D., and J. A. White. 2005. Channel noise is essential for perithreshold oscillations in entorhinal stellate neurons. *J. Neurosci.* 25:10025–10028.
73. Cox, C. D., J. M. McCollum, …, M. L. Simpson. 2006. Frequency domain analysis of noise in simple gene circuits. *Chaos.* 16:026102.
74. Bezrukov, S. M., and I. Vodyanoy. 1995. Noise-induced enhancement of signal transduction across voltage-dependent ion channels. *Nature.* 378:362–364.
75. Ries, J., and P. Schwille. 2012. Fluorescence correlation spectroscopy. *BioEssays.* 34:361–368.
76. Fill, M., and J. A. Copello. 2002. Ryanodine receptor calcium release channels. *Physiol. Rev.* 82:893–922.
77. Lanner, J. T., D. K. Georgiou, …, S. L. Hamilton. 2010. Ryanodine receptors: structure, expression, molecular details, and function in calcium release. *Cold Spring Harb. Perspect. Biol.* 2:a003996.
78. Gardiner, C. 2009. Stochastic Methods: A Handbook for the Natural and Social Sciences. Springer, Berlin, Germany.
79. Gillespie, D. T. 2000. The chemical Langevin equation. *J. Chem. Phys.* 113:297–306.
80. Berridge, M. J. 2006. Calcium microdomains: organization and function. *Cell Calcium.* 40:405–412.
81. Xu, T., X. Yu, …, Y. Zuo. 2009. Rapid formation and selective stabilization of synapses for enduring motor memories. *Nature.* 462:915–919.
82. Bers, D. M. 2002. Cardiac excitation-contraction coupling. *Nature.* 415:198–205.